

# An Experimental Study of Acoustically Enhanced NAPL Dissolution in Porous Media

Eric T. Vogler and Constantinos V. Chrysikopoulos

Dept. of Civil and Environmental Engineering, University of California, Irvine, CA, 92697

DOI 10.1002/aic.10221

Published online in Wiley InterScience (www.interscience.wiley.com).

*The effects of acoustic waves on the dissolution of dense nonaqueous phase liquids in water saturated porous media are investigated. Experiments of trichloroethylene (TCE) ganglia dissolution within a water saturated column, packed with glass beads, are conducted. Acoustic waves with pressure amplitudes ranging from 0 to 1625 Pa and frequencies ranging from 0 to 285 Hz are employed to the interstitial fluid at the inlet of the packed column. Effluent dissolved TCE concentrations are observed to increase up to 120% in the presence of acoustic pressure waves compared to the case where TCE dissolution without acoustic waves is monitored. The observed effluent dissolved TCE concentration increase is attributed to enhanced mass flux at the TCE-water interface, caused by acoustic waves. Highest dissolution rates occur at discrete frequencies suggesting resonance effects or the presence of standing waves. Although acoustic waves enhance TCE dissolution, they dissipate almost exponentially with distance from the acoustic source. © 2004 American Institute of Chemical Engineers AIChE J, 50: 3271–3280, 2004*  
*Keywords: Contaminant transport, NAPL dissolution, acoustic waves, enhanced mass transfer, aquifer remediation*

## Introduction

The removal of nonaqueous phase liquids (NAPLs) from groundwater aquifers is a challenging task, because these liquids are only slightly soluble in water (Mercer and Cohen, 1990) making their dissolution very slow and mass-transfer limited (Chrysikopoulos et al., 1994; Khachikian and Harmon, 2000). Unfortunately, only a few parts per billion of certain contaminants such as trichloroethylene (TCE) can render groundwater nonpotable. Consequently, removing NAPL sources from groundwater aquifers is essential for protecting human health.

Currently, there is a strong interest in alternative aquifer remediation procedures because the most commonly used remediation technique, pump-and-treat, is not capable of removing residual dense nonaqueous phase liquid (DNAPL) sources from contaminated aquifers (Wilson et al., 1990). Alternative

remediation methods include the use of cosolvents which enhance dissolution by chemically altering the groundwater (Brandes and Farley, 1993). A closely related aquifer remediation technology involves the use of surfactants that can reduce the surface tension and also enhance the dissolution and mobilization of DNAPLs (Pennel et al., 1993; Mason and Kueper, 1996; Fortin et al., 1997). Another method is bioremediation, which uses bacteria to enhance NAPL degradation (Chaudhry, 1994; Seagren et al., 1994). The addition of humic substances, which enhance NAPL dissolution in saturated porous media, has also been investigated (Tatalovich et al., 2000). All of these remediation methods, however, have the disadvantage of introducing further contamination into the subsurface.

The use of acoustic waves and/or vibration have been proposed as potential groundwater remediation techniques. Several studies suggested that vibration of porous media can mobilize NAPL ganglia (Reddi and Wu, 1996; Reddi et al., 1998). Pressure pulsing has been found to enhance the mobilization and extraction of oil in porous media (Dusseault et al., 2000). Axial stress applied to the face of a TCE contaminated sand core has been shown to enhance TCE droplet production in the

Correspondence concerning this article should be addressed to C. V. Chrysikopoulos at costas@eng.uci.edu.

effluent stream (Roberts et al., 2001). Resonant behavior of saturated porous media, neglecting motion of porous media parallel to the flow of the interstitial fluid, has been determined to be a function of porosity (Pan and Horne, 2000). A recent experimental study has also shown that acoustic waves enhance solute transport in saturated porous media due to the addition of an oscillatory interstitial water velocity to the background flow field (Vogler and Chrysikopoulos, 2002). The additional oscillatory interstitial flow velocity is caused in part by an out of phase pressure wave (slow wave) compared to the motion of the solid matrix (Biot, 1956a,b). A theoretical analysis of slow wave decay in a poroelastic medium has been presented by Zimmerman and Stern (1994).

Several studies suggest that NAPL dissolution in saturated porous media is positively dependent on the interstitial water velocity (Imhoff et al., 1994; Powers et al., 1994; Chrysikopoulos et al., 2000; Lee and Chrysikopoulos, 2002; Dela Barre et al., 2002; Seagren and Moore, 2003; Nambi and Powers, 2003; Chrysikopoulos et al., 2003, to mention a few). Consequently, it is reasonable to expect that acoustic waves can lead to dissolution enhancement of residual DNAPLs in porous media. A novel "clean" remediation method is proposed and investigated in this study. The method uses acoustic waves to enhance DNAPL dissolution rates by increasing the NAPL-water interphase mass transfer.

## Mathematical Developments

Acoustic wave propagation through one-dimensional (1-D), water saturated porous media, assuming the interstitial fluid and solid beads (packing) are incompressible, may be described by the following two equations that account for the motion of the interstitial fluid and solid matrix, and a mass conservation equation (de Boer et al., 1993)

$$(\lambda + 2\mu) \frac{\partial^2 \xi_s(t, x)}{\partial x^2} - (1 - \theta) \frac{\partial p(t, x)}{\partial x} - \rho_s \frac{\partial^2 \xi_s(t, x)}{\partial t^2} + S \left[ \frac{\partial \xi_f(t, x)}{\partial t} - \frac{\partial \xi_s(t, x)}{\partial t} \right] = 0 \quad (1)$$

$$-\theta \frac{\partial p(t, x)}{\partial x} - \rho_f \frac{\partial^2 \xi_f(t, x)}{\partial t^2} - S \left[ \frac{\partial \xi_f(t, x)}{\partial t} - \frac{\partial \xi_s(t, x)}{\partial t} \right] = 0 \quad (2)$$

$$(1 - \theta) \frac{\partial^2 \xi_s(t, x)}{\partial t \partial x} + \theta \frac{\partial^2 \xi_f(t, x)}{\partial t \partial x} = 0 \quad (3)$$

where  $\mu$  and  $\lambda$  are the solid matrix Lamé constants, representing the shear modulus and the bulk modulus less 2/3 of the shear modulus, respectively;  $\xi_s$  is the solid displacement;  $\xi_f$  is the fluid displacement;  $x$  is the spatial coordinate in the direction of flow;  $\theta$  is the fluid volume fraction or porosity of the porous medium;  $(1 - \theta)$  is the volume fraction of solids per unit volume of the porous medium;  $p$  denotes fluid pressure;  $t$  is time;  $\rho_s = (1 - \theta) \rho_{\text{solid}}$  is the solid bulk density (where  $\rho_{\text{solid}}$  is the solid density);  $\rho_f = \theta \rho_{\text{H}_2\text{O}}$  is the fluid bulk density (where  $\rho_{\text{H}_2\text{O}}$  is the water density);  $S$  is a function that relates the extra stress due to the relative movement between the solid and fluid (de Boer and Ehlers, 1990)

$$S = \frac{\theta^2 \gamma}{K} \quad (4)$$

where  $\gamma$  is the specific weight of the fluid; and  $K$  is the hydraulic conductivity of the porous medium. The preceding expression for  $S$  is valid only under Poiseuille flow conditions. The breakdown of Poiseuille flow at specified kinematic fluid viscosity,  $\eta$  and mean pore diameter occurs beyond a threshold frequency. For pore diameters in the range 0.1 to 0.01 mm, the corresponding range of threshold frequencies, at 15°C, is 100 to 10,000 Hz (Biot, 1956a).

Assuming that there is no initial displacement or velocity for the fluid and solid matrix, the appropriate initial conditions considered here are

$$\xi_s(0, x) = \xi_f(0, x) = 0 \quad (5)$$

$$\frac{\partial \xi_s(0, x)}{\partial t} = \frac{\partial \xi_f(0, x)}{\partial t} = 0 \quad (6)$$

Furthermore, assuming that the porous medium is semi-infinite, the boundary conditions for the solid and fluid phases are given by

$$\sigma(t, 0) = (1 - \theta) f(t) = (2\mu + \lambda) \frac{d\xi_s}{dx} \quad (7)$$

$$\sigma(t, \infty) = p(t, \infty) = 0 \quad (8)$$

where  $\sigma$  is solid stress caused by the interaction between solid and fluid movement (de Boer et al., 1993) and  $f(t)$  is an acoustic pressure source function. The boundary condition (Eq. 7) equates the stress of the solid matrix and the pressure of the fluid at the acoustic source boundary.

The solution to the boundary value mathematical problem described is obtained with the methods of de Boer et al. (1993) who have examined the governing differential Eqs. 1–3 for a different set of boundary conditions. Taking Laplace transforms of Eqs. 1–3, with respect to time variable  $t$ , and employing initial conditions (Eqs. 5 and 6), leads to the following set of equations

$$(\lambda + 2\mu) \frac{d^2 \tilde{\xi}_s(v, x)}{dx^2} - (1 - \theta) \frac{d\tilde{p}(v, x)}{dx} - (\rho_s v^2 + S v) \tilde{\xi}_s(v, x) + S v \tilde{\xi}_f(v, x) = 0 \quad (9)$$

$$-\theta \frac{d\tilde{p}(v, x)}{dx} - (\rho_f v^2 + S v) \tilde{\xi}_f(v, x) + S v \tilde{\xi}_s(v, x) = 0 \quad (10)$$

$$(1 - \theta) v \frac{d\tilde{\xi}_s(v, x)}{dx} + \theta v \frac{d\tilde{\xi}_f(v, x)}{dx} = 0 \quad (11)$$

where the "tilde" signifies Laplace transform defined as

$$L[\beta(t)] = \tilde{\beta}(v) = \int_0^{\infty} \beta e^{-vt} dt \quad (12)$$

$\beta$  is a dummy variable, and  $v$  is the Laplace transform parameter. Placing Eq. 9 through 11 into matrix notation results in

$$\mathbf{F} \frac{d^2 \mathbf{m}}{dx^2} + \mathbf{G} \frac{d \mathbf{m}}{dx} + \mathbf{H} \mathbf{m} = \mathbf{0} \quad (13)$$

where

$$\mathbf{m} = [\tilde{\xi}_s(v, x), \tilde{\xi}_f(v, x), \tilde{p}(v, x)]^T \quad (14)$$

the superscript T indicates transpose, and matrices  $\mathbf{F}$ ,  $\mathbf{G}$ , and  $\mathbf{H}$  are

$$\mathbf{F} = \begin{bmatrix} \lambda + 2\mu & 0 & 0 \\ 0 & 0 & 0 \\ 0 & 0 & 0 \end{bmatrix} \quad (15)$$

$$\mathbf{G} = \begin{bmatrix} 0 & 0 & -(1-\theta) \\ 0 & 0 & -\theta \\ (1-\theta)v & \theta v & 0 \end{bmatrix} \quad (16)$$

$$\mathbf{H} = \begin{bmatrix} -\rho_f v^2 - Sv & Sv & 0 \\ Sv & -\rho_f v^2 - Sv & 0 \\ 0 & 0 & 0 \end{bmatrix} \quad (17)$$

Assuming a trial solution for  $\mathbf{m}$  in the form

$$\mathbf{m} = \mathbf{m}_0 e^{\alpha x} \quad (18)$$

where  $\mathbf{m}_0$  and  $\alpha$  are functions of the Laplace transform parameter  $v$ . Substitution of Eq. 18 into 13 results in the following eigenvalue problem

$$(\alpha^2 \mathbf{F} + \alpha \mathbf{G} + \mathbf{H}) \mathbf{m}_0 e^{\alpha x} = \mathbf{0} \quad (19)$$

The eigenvalues are determined from the characteristic equation

$$|\alpha^2 \mathbf{F} + \alpha \mathbf{G} + \mathbf{H}| = \alpha^2 \{(\lambda + 2\mu)\theta^2 \alpha^2 - [(1-\theta)^2 \rho_f + \theta^2 \rho_s] v^2 - Sv\} = 0 \quad (20)$$

where the latter formulation in the preceding expression is the consequence of substitution of Eq. 15–17, followed by determinant evaluation. The roots or eigenvalues of the characteristic equation are

$$\alpha_1 = (\Omega_1 v^2 + \Omega_2 v)^{1/2} \quad (21)$$

$$\alpha_2 = -(\Omega_1 v^2 + \Omega_2 v)^{1/2} \quad (22)$$

$$\alpha_3 = \alpha_4 = 0 \quad (23)$$

where

$$\Omega_1 = \frac{(1-\theta)^2 \rho_f + \theta^2 \rho_s}{(\lambda + 2\mu)\theta^2} \quad (24)$$

$$\Omega_2 = \frac{S}{(\lambda + 2\mu)\theta^2} \quad (25)$$

Consequently, the corresponding eigenvectors are

$$\mathbf{q}_1 = \left[ \frac{-\theta}{(1-\theta)}, 1, \frac{-(1-\theta)\rho_f v^2 - Sv}{(1-\theta)\theta(\Omega_1 v^2 + \Omega_2 v)^{1/2}} \right]^T \quad (26)$$

$$\mathbf{q}_2 = \left[ \frac{-\theta}{(1-\theta)}, 1, \frac{(1-\theta)\rho_f v^2 + Sv}{(1-\theta)\theta(\Omega_1 v^2 + \Omega_2 v)^{1/2}} \right]^T \quad (27)$$

$$\mathbf{q}_3 = \mathbf{q}_4 = [0, 0, 1]^T \quad (28)$$

The Laplace domain solution can be expressed as

$$\mathbf{m} = A_1 \mathbf{q}_1 e^{\alpha_1 x} + A_2 \mathbf{q}_2 e^{\alpha_2 x} + A_3 \mathbf{q}_3 + A_4 x \mathbf{q}_4 \quad (29)$$

where  $A_1, \dots, A_4$  are the Laplace domain constants to be determined. In view of boundary condition (Eq. 8), it is evident that the solution can be finite at  $x \rightarrow \infty$  only if  $A_1 = A_4 = 0$ . Thus, the Laplace domain solution reduces to

$$\mathbf{m} = A_2 \mathbf{q}_2 e^{\alpha_2 x} + A_3 \mathbf{q}_3 \quad (30)$$

In view of Eq. 14, 27, 28, and boundary condition (Eq. 7), the constants  $A_2$  and  $A_3$  are determined as

$$A_2 = \tilde{f}(v) \frac{(1-\theta)^2}{\theta(\lambda + 2\mu)(\Omega_1 v^2 + \Omega_2 v)^{1/2}} \quad (31)$$

$$A_3 = \tilde{f}(v) \left[ \theta - \frac{(1-\theta)^2 \rho_f v^2 + (1-\theta)Sv}{\theta^2(\lambda + 2\mu)(\Omega_1 v^2 + \Omega_2 v)} \right] \quad (32)$$

Consequently, the Laplace domain solutions for  $\tilde{\xi}_s(v, x)$ ,  $\tilde{\xi}_f(v, x)$  and  $\tilde{p}_f(v, x)$  can be expressed as

$$\tilde{\xi}_s(v, x) = \frac{(\theta-1)}{(2\mu + \lambda)} \tilde{f}(v) \tilde{\Psi}(v, x) \quad (33)$$

$$\tilde{\xi}_f(v, x) = \frac{(1-\theta)^2}{\theta(2\mu + \lambda)} \tilde{f}(v) \tilde{\Psi}(v, x) \quad (34)$$

$$\tilde{p}_f(v, x) = \{\exp[-(\Omega_1 v^2 + \Omega_2 v)^{1/2} x] - 1\} \tilde{f}(v) \tilde{\Phi}(v, x) + \theta \tilde{f}(v) \quad (35)$$

where

$$\tilde{\Psi}(v, x) = \frac{\exp[-(\Omega_1 v^2 + \Omega_2 v)^{1/2} x]}{(\Omega_1 v^2 + \Omega_2 v)^{1/2}} \quad (36)$$

$$\tilde{\Phi}(\nu, x) = \frac{(1 - \theta)^2 \rho_f \nu^2 + (1 - \theta) S \nu}{\theta^2 (\lambda + 2\mu) (\Omega_1 \nu^2 + \Omega_2 \nu)} \quad (37)$$

Taking the Laplace inverse transformation of Eq. 33 – 35 yields

$$\xi_s(t, x) = \frac{(\theta - 1)}{\Omega_1^{1/2} (\lambda + 2\mu)} \int_0^t f(t - \tau) \exp\left[-\frac{\Omega_2 \tau}{2\Omega_1}\right] \times I_0\left[\frac{\Omega_2(\tau^2 - \Omega_1 x^2)^{1/2}}{2\Omega_1}\right] H(\tau - \Omega_1^{1/2} x) d\tau \quad (38)$$

$$\xi_s(t, x) = \frac{(1 - \theta)^2}{\Omega_1^{1/2} \theta (\lambda + 2\mu)} \int_0^t f(t - \tau) \exp\left[-\frac{\Omega_2 \tau}{2\Omega_1}\right] \times I_0\left[\frac{\Omega_2(\tau^2 - \Omega_1 x^2)^{1/2}}{2\Omega_1}\right] H(\tau - \Omega_1^{1/2} x) d\tau \quad (39)$$

$$p(t, x) = \frac{(1 - \theta)}{\theta^2 (\lambda + 2\mu)} \left[ (1 - \theta) \rho_f \frac{\partial^2 \Lambda(t, x)}{\partial t^2} + S \frac{\partial \Lambda(t, x)}{\partial t} \right] + \theta p_s \sin(\omega t), \quad (40)$$

$$\Lambda(t, x) = \int_0^t Q(t - \tau) G(\tau, x) d\tau \quad (41)$$

$$Q(t) = \Omega_1^{-1/2} \int_0^t f(t - \tau) \exp\left[-\frac{\Omega_2 \tau}{2\Omega_1}\right] I_0\left[-\frac{\Omega_2 \tau}{2\Omega_1}\right] d\tau \quad (42)$$

$$G(t, x) = \Omega_1^{-1/2} \exp\left[-\frac{\Omega_2 t}{2\Omega_1}\right] \times \left\{ I_0\left[\frac{\Omega_2(t^2 - \Omega_1 x^2)^{1/2}}{2\Omega_1}\right] H(t - \Omega_1^{1/2} x) - I_0\left[-\frac{\Omega_2 t}{2\Omega_1}\right] \right\} \quad (43)$$

where the following Laplace inversion identities were utilized (Abramowitz and Stegun, 1965)

$$L^{-1}\{\tilde{g}_1(\nu) \tilde{g}_2(\nu)\} = \int_0^t g_1(\tau) g_2(t - \tau) d\tau \quad (44)$$

$$L^{-1}\{\tilde{\Psi}(\nu, x)\} = \Omega_1^{-1/2} \exp\left[-\frac{\Omega_2}{2\Omega_1} t\right] \times I_0\left[\frac{\Omega_2(t^2 - \Omega_1 x^2)^{1/2}}{2\Omega_1}\right] H(t - \Omega_1^{1/2} x) \quad (45)$$

where  $L^{-1}$  is the Laplace inverse operator,  $I_0$  is the modified Bessel function of zero-order, and  $H$  is the unit step function or Heaviside function.

The fluid displacement relative to the solid displacement may be written as

$$\xi_r(t, x) = \xi_f(t, x) - \xi_s(t, x) \quad (46)$$

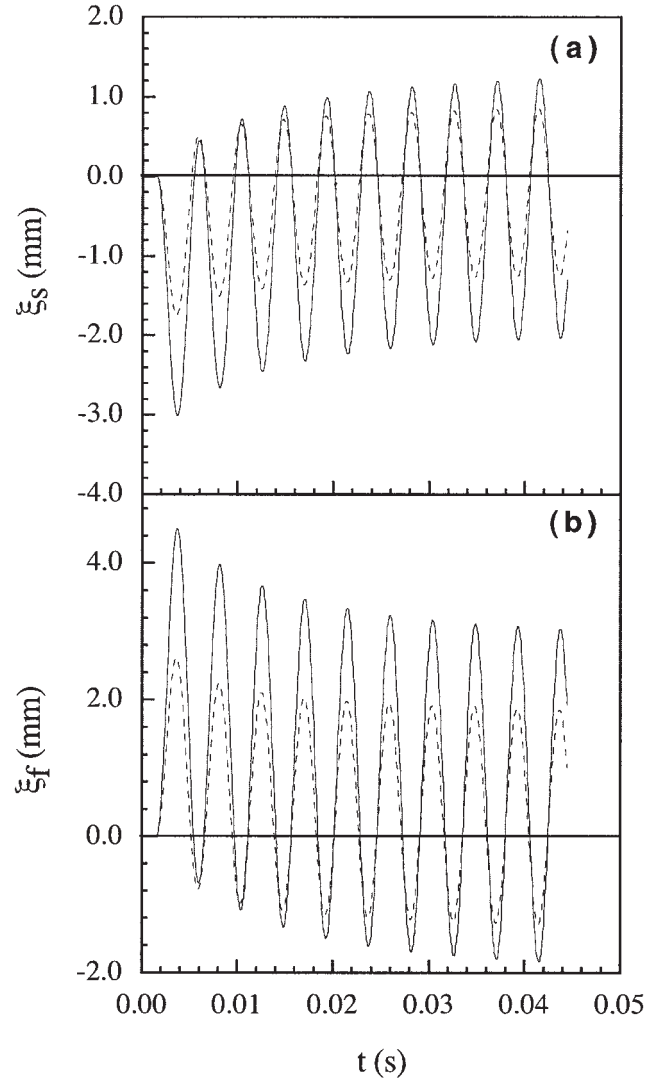


**Figure 1. Simulated (a) solid, and (b) fluid displacements as a function of time at  $x=0.15$  m for an acoustic wave source with  $\phi=225$  Hz, and  $p_s = 1$  kPa.**

Dashed and solid curves represent column packings of 1 and 2 mm size beads, respectively.

Furthermore, a time and space dependent relative fluid velocity  $U_r(t, x)$ , may be determined by differentiating Eq. 46 with respect to time. Because  $U_r(t, x) = d\xi_r(t, x)/dt$  is a function of acoustic pressure and frequency which may vary between different experiments, the acoustic Reynolds number (Ha and Yavuzkurt, 1993a,b)

$$Re_a = \frac{U_{r,a} d}{\eta} \quad (47)$$

where  $U_{r,a}$  is the maximum value or amplitude of the oscillatory interstitial pore water velocity over one period of oscillation ( $1/\phi$ , where  $\phi$  is the acoustic wave frequency), and  $d$  is the mean grain diameter of the porous medium that will be used in this study for consistent comparison of our experimental data.

Figure 1 presents model simulations for both fluid and solid

**Table 1. Column Packing Material and Fluid Properties**

Parameter	Value
$K^\dagger$	0.06 m/s (1 mm beads)
$K^\dagger$	0.25 m/s (2 mm beads)
$\theta$	0.40
$(1-\theta)$	0.60
$\rho_{H_2O}$	1000.0 Kg/m <sup>3</sup>
$\rho_{bead}$	2330.0 Kg/m <sup>3</sup>
$\rho_f$	400.0 Kg/m <sup>3</sup>
$\rho_s$	1398.0 Kg/m <sup>3</sup>
$\eta^\ddagger$	$1.0037 \times 10^{-6}$ m <sup>2</sup> /s
$\lambda^\ddagger$	$5.5833 \times 10^6$ N/m <sup>2</sup>
$\mu^\ddagger$	$8.375 \times 10^6$ N/m <sup>2</sup>
$\gamma$	$1.0 \times 10^5$ N/m <sup>3</sup>

<sup>†</sup>For water at 20°C.

<sup>‡</sup>Adopted from de Boers et al. (1993).

displacements in 1-D, water saturated porous media with  $d = 1$  mm (dashed curves) and  $d = 2$  mm (solid curves) for the following acoustic source function

$$f(t) = p_s \sin(\omega t) \quad (48)$$

where  $p_s$  is the acoustic source fluid pressure, and  $\omega = 2\pi\phi$  is the angular frequency. The curves are generated with the analytical solutions for  $\xi_s(t, x)$  and  $\xi_f(t, x)$  in Eqs. 38 and 39, respectively, where the integrals were evaluated numerically with IMSL subroutine *dqdag* (IMSL, 1991). All of the model parameters employed are listed in Table 1. The displacements are evaluated at a location  $x=0.15$  m downstream from the acoustic source with  $p_s=1$  kPa and  $\theta=225$  Hz. Note that positive ( $\xi_s, \xi_f > 0$ ) and negative ( $\xi_s, \xi_f < 0$ ) displacements refer to directions away and toward the acoustic source, respectively. The simulated solid displacements for the case of 2 mm beads are shown to be greater than for the case of 1 mm beads (Figure 1a). The same trend is observed in the simulations of the fluid displacement (Figure 1b). This is attributed to the decreasing value of  $S$  (see Eq. 4) with increasing hydraulic conductivity. As  $S$  decreases, the exponential term in Eq. 38 and 39 increases, causing  $\xi_s$  and  $\xi_f$  to increase. The hydraulic conductivity is greater for the 2 mm beads. Consequently, there is less friction between the pore fluid and the solid matrix of the packed column. Comparison of Figures 1a and 1b indicates that the magnitude of the fluid displacement is greater than that of the solid displacement. In addition, the equilibrium position, which refers to the position of the center of the oscillatory displacement, is initially located toward the acoustic source (negative displacement) for  $\xi_s$ , and away from the acoustic source (positive displacement) for  $\xi_f$ . However, the equilibrium positions for both  $\xi_s$  and  $\xi_f$  are progressively (asymptotically) shifted toward the zero displacement position ( $\xi_s = \xi_f = 0$ ). It should be noted that only the amplitude of  $\xi_s$  and  $\xi_f$  is important in determining  $U_r$ . The porous medium and pore fluid continue to oscillate harmonically with time as long as the acoustic source pressure is applied.

The dependence of  $Re_a$  on the distance from the acoustic source, acoustic wave frequency, and acoustic source fluid pressure is illustrated in Figure 2. The parameter  $U_r$ , present in the  $Re_a$  expression (Eq. 47), is obtained by numerical approximation of the derivative  $d\xi_f(t, x)/dt$  and evaluation of its maximum value over a period of acoustic wave oscillation,

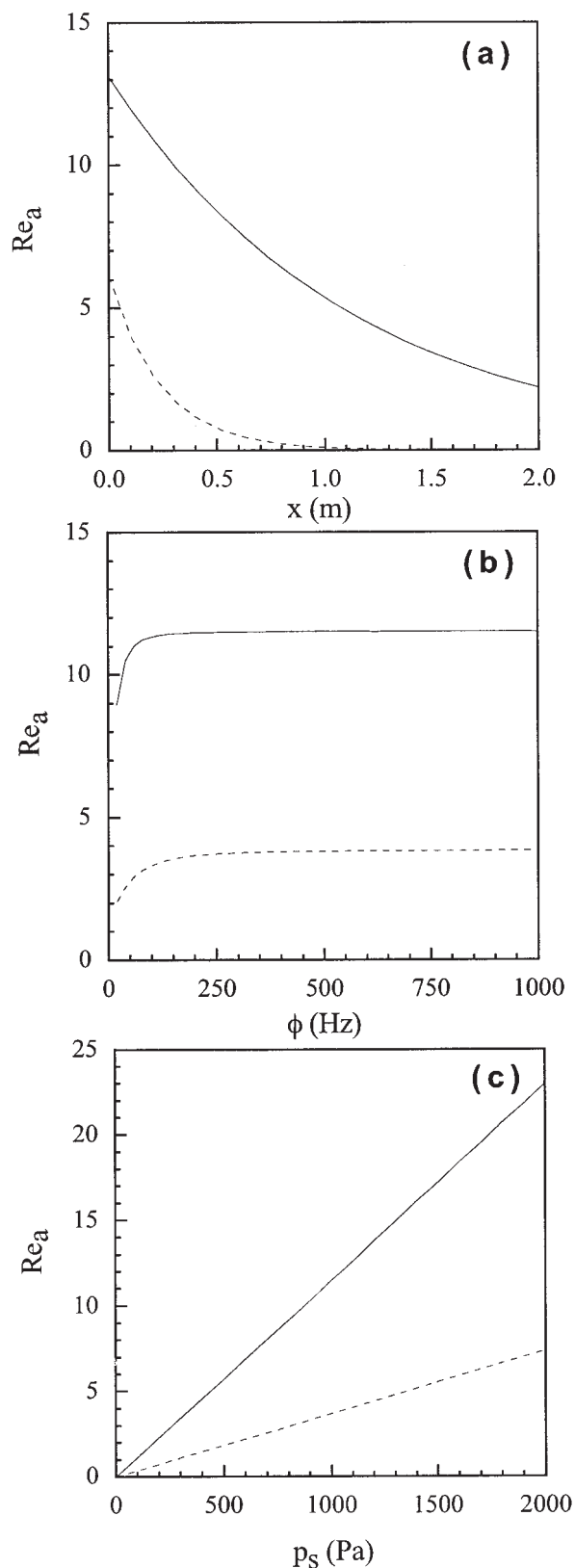


**Figure 2. Acoustic Reynolds number as a function of (a)  $x$ , (b)  $\phi$ , and (c)  $p_s$  (here  $x=0.15$  m,  $\phi= 225$  Hz,  $p_s = 1$  kPa).**

Dashed and solid curves represent column packings of 1 and 2 mm size beads, respectively.

$1/\phi$ . The term  $\xi_s(t, x)$  is evaluated from Eq. 46 with  $\xi_s(t, x)$  and  $\xi_f(t, x)$  provided by the theoretically derived expressions in Eqs. 38 and 39, respectively. The simulations in Figure 2a indicate that  $Re_a$  decreases with increasing  $x$ . Figure 2b shows that  $Re_a$  reaches an asymptotic value with increasing  $\phi$ . Figure 2c shows that  $Re_a$  increases linearly with increasing  $p_s$ . It should be noted that the  $Re_a$  values are consistently higher for  $d = 2$  mm (solid curves) than  $d = 1$  mm (dashed curves). This is attributed to greater hydraulic conductivities and, consequently, less viscous losses in the column with the greater bead-size packing, due to smaller total bead surface areas per unit volume.

Although,  $Re_a$  decreases rapidly with increasing distance from the acoustic source (Figure 2a), it is linearly proportional to  $p_s$  (Figure 2c). Note that the acoustic source pressure used to construct Figure 2a is only 1 kPa. However, for field scale applications, greater  $Re_a$  may be achieved at greater distances from the acoustic source by increasing  $p_s$ . For certain field applications,  $p_s$  can exceed 400 kPa if formation compressibility is such that inelastic compaction of the porous medium is avoided. Acoustic source devices capable of delivering substantial acoustic pressures should be used for field scale applications.

## Experimental Procedures

The effect of acoustic pressure waves on mass transfer from a DNAPL blob in saturated porous media was investigated by conducting flow through dissolution experiments in a 30 cm long glass laboratory column with a 2.5 cm inner diameter (Kimble Kontes, NJ). The column was packed with either 1 or 2 mm dia. soda lime glass beads with a density of 2.33 g/cm<sup>3</sup> (Fisher Scientific, PA). The porosity of the column packed with 1 or 2 mm glass beads is approximately 0.4. This experimentally determined porosity value is in agreement with values published in the literature for loose random packing obtained by dropping glass beads into a column as a loose mass (de Klerk, 2003). Relatively large glass beads, in comparison to the column diameter, were employed in order to achieve the greatest possible transmission of acoustic pressure waves through the packed column. However, bed voidance for column to particle diameter ratios greater than 11.2 has been shown experimentally to be relatively constant (de Klerk, 2003). The beads were retained in the column using Teflon screens and end caps on both the influent and effluent sides of the column. The Teflon column end caps were milled to accommodate 1/4 in. stainless steel fittings (Swageloc) for 3/8 in. semirigid plastic tubing (Fisher Scientific, PA). Constant flow of degassed Millipore water at 3.25 mL/min, corresponding to an interstitial pore velocity of 1.66 cm/min and 0.0552 pore volumes/min, was maintained through the packed column with a microprocessor pump drive (Cole Palmer Instrument Co., IL). Acoustic pressure was introduced into the column with a custom designed acoustic reservoir containing a pressure transducer (TST37; Clark Synthesis, CO). The frequency of the acoustic pressure oscillation was controlled by a frequency generator (LG Precision, CA). Acoustic pressure levels were controlled by an amplifier (Lab Gruppen, Sweden) and measured using PCB106b pressure sensors (PCB Piezotronics, Inc., NY). One pressure sensor was installed in the acoustic reservoir to measure the acoustic source pressure. Another sensor was placed in

the effluent line, just after the packed column, to measure the effluent pressure as close to the packed column as possible. Pressure sensor measurements were made using a signal conditioner (PCB Piezotronics, Inc., NY) in addition to a digital multimeter (Metex, Korea) and oscilloscope (EZ Digital Co., Ltd., Korea). A complete experimental apparatus is shown in Figure 3.

Effluent samples (0.15 mL) were collected from a dedicated needle within the effluent tube (sample port) at regular 10 min intervals (a time period required for 0.55 pore volumes of interstitial fluid to pass through the packed column) using disposable 1.0 mL of tuberculin plastic syringes (Becton Dickinson & Co., NJ). The samples were immediately introduced into 2-mL vials (Kimble Glass, NJ) containing a known volume of n-pentane (Fisher Scientific, PA). The TCE concentrations of the liquid samples were determined using a Hewlett Packard 5890 Series II gas chromatograph with an electron capture detector.

DNAPL dissolution experiments were initiated by injecting 0.05 mL of TCE (Fisher Scientific, PA) dyed red with oil red EGN (Aldrich Chemical Co., WI) into a side injection port in the middle of the packed column and allowed to equilibrate to flow conditions within the packed column. Preliminary TCE dissolution experiments, in the absence of acoustic waves (base case), suggested that 5 pore volumes were sufficient to achieve relatively steady effluent concentrations. Moreover, it was observed that the effluent concentration remained relatively constant for over 30 pore volumes, greatly exceeding the time-scale of the experiments performed in this study. To assess the effect of acoustic waves on NAPL dissolution, a range of acoustic frequencies and amplitudes were applied at 60 min intervals following a 120 min period of flow without acoustic pressure.

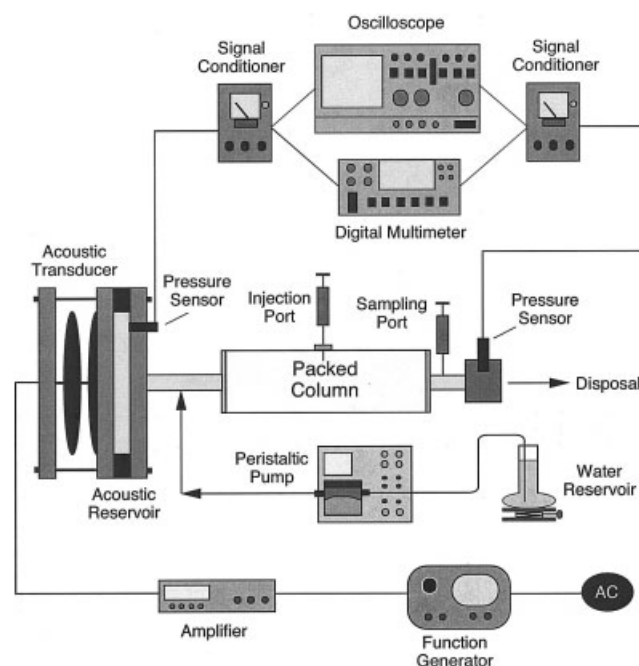
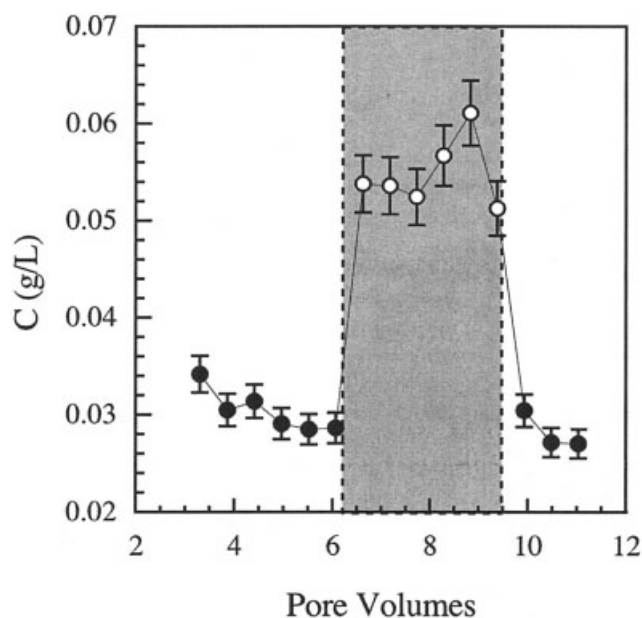


Figure 3. Experimental setup.



**Figure 4.** Effluent dissolved TCE concentrations from a column packed with 2 mm beads in the presence (shaded area) and absence of acoustic waves (here  $x=0.15$  m,  $\phi=225$  Hz,  $p_s=812$  Pa).

Solid circles represent the base case (no acoustic pressure) and open circles in the grey shaded region represent portions of the experiment where acoustic waves are present. The bars indicate experimental error.

## Results and Discussion

Dissolution experiments were conducted with acoustic wave frequencies ranging from 0 (base case) to 285 Hz using a constant acoustic source fluid pressure amplitude of  $p_s=812$  Pa. Two columns packed with 1 and 2 mm beads, respectively, were employed. Experiments were also conducted using a constant acoustic wave frequency of  $\phi=245$  Hz with acoustic source fluid pressures ranging from 0 (base case) to 1,625 Pa. The acoustic frequencies and the column packing employed in this study were carefully selected so that threshold frequencies were never exceeded and Eq. 4 is always valid. A set of experimental data for the 2 mm bead column packing with  $p_s=812$  Pa at  $\phi=225$  Hz are presented in Figure 4. The dissolved TCE effluent concentration is observed to increase significantly during the generation of acoustic waves, as shown in the shaded area of Figure 4. It should also be noted that effluent concentrations return to their original base case values after discontinuing the acoustic pressure for approximately three pore volumes. The enhanced dissolution observed is attributed to small scale displacement oscillations. These oscillations are responsible for an oscillatory pore water velocity that is sufficient to change the pore-scale concentration gradient over the individual TCE-water interfacial areas.

A second acoustic wave mechanism that could have contributed to the enhancement of dissolved TCE effluent concentrations may be a physical change in the injected TCE blob configuration, which was observed in previous vibration studies (Reddi et al., 1998). This change in DNAPL blob configuration is referred to as the snap-off mechanism which causes DNAPL blobs to snap-off in individual pore bodies and con-

sequently leads to increased DNAPL-water interfacial areas (Chatzis et al., 1983; Mohanty et al., 1987; Morrow et al., 1988). Effluent concentrations are observed to return to base case values as soon as acoustic pressures were discontinued (see Figure 4). Although snap-off may occur as the DNAPL blobs dissolve with or without acoustic enhancement, it would not be noticeable within the time-scale of the experiments conducted in this work. Nonetheless, the observed increase in the effluent concentrations is mainly attributed to the presence of the acoustic waves and not to permanent changes in the geometry of the DNAPL blobs due to snap-off.

In order to clearly present in a single plot the results from the various TCE dissolution experiments conducted in this study, the experimental data are expressed as the average percent change in effluent concentration

$$\Delta C = \frac{\bar{C}_a - \bar{C}_b}{\bar{C}_b} \quad (49)$$

where  $\bar{C}_a$  is the average of the effluent concentrations determined for the last 3 samples (1.66 pore volumes) collected in the presence of acoustic waves from each TCE dissolution experiment, and  $\bar{C}_b$  is the average of the last 3 samples collected in the absence of acoustic waves. The complete set of the experimental data collected are shown in Figure 5a and in Table 2. Note that each symbol in Figure 5a represents a different TCE dissolution experiment. The greatest observed change in effluent dissolved TCE concentration due to the addition of acoustic waves is  $\Delta C = 120$ , and 96% for the 1 and 2 mm bead column packings, respectively, and occurs at  $\phi=225$  Hz. Another major  $\Delta C$  peak occurs at  $\phi=161$  Hz. The cause of the observed  $\Delta C$  peaks may be attributed to different pressures within the packed column. Although a constant acoustic source fluid pressure of  $p_s = 812$  Pa is employed here, as shown in Figure 5b, the effluent fluid pressures  $p_e$  are not constant for the different frequencies used. It should also be noted that  $\Delta C$  is consistently greater for 1 mm beads than the 2 mm beads. This is attributed to greater TCE-water interfacial areas associated with the smaller bead-size column packing.

Comparison of Figures 5a and 5b shows that  $p_e$  follows the same trend as  $\Delta C$ . The effluent fluid pressures are greater for the 1 mm bead than 2 mm bead-size column packing. A possible explanation for this is that the observed  $p_e$  peaks for the different  $\phi$  values employed with constant  $p_s$  may be caused by the presence of standing waves that can lead to location dependent acoustic pressure. Furthermore, the fact that the highest dissolution rates occur at discrete frequencies suggest a resonance effect. The formation of standing waves and the occurrence of resonance effects are mainly dependent on the physical geometry and boundaries of the experimental packed column. Although the theoretical developments presented here adequately relate the experimental dissolution data to the different acoustic wave frequencies and pressures, they do not account for the presence of standing waves or resonant frequencies.

The effect of the acoustic source fluid pressure for a constant frequency of  $\phi=245$  Hz on  $\Delta C$  is shown in Figure 6, where the dotted and solid lines are the best linear fits for columns packed with 1 and 2 mm beads, respectively. Clearly,  $\Delta C$  increases with increasing  $p_s$ . Furthermore, with the exception of the data

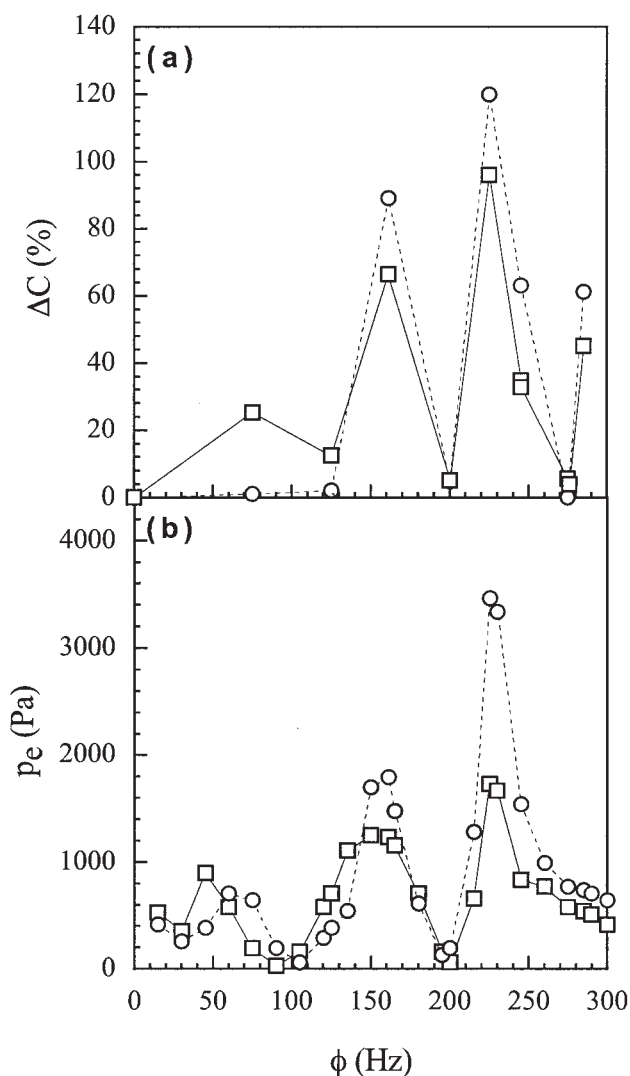


**Figure 5. Effect of  $\phi$  on (a) percent change in effluent dissolved TCE concentration, and (b) effluent fluid pressure (here  $x=0.15$  m,  $p_s=812$  Pa).**

Circles with dashed lines and squares with solid lines represent column packings of 1 and 2 mm size beads, respectively.

collected at  $p_s = 1,625$  Pa,  $\Delta C$  is greater for the column packed with 1 mm beads than 2 mm beads. Note that two experiments were performed with the column packed with 2 mm beads at  $p_s = 812$  Pa, and the results were practically identical. This is an indication of the good experimental reproducibility.

Figure 7 illustrates the effect of  $\phi$  and  $p_s$  expressed as  $Re_a$  on  $\Delta C$ . The dotted and solid lines correspond to the best linear fits for columns packed with 1 and 2 mm beads, respectively. Clearly, the results suggest that the TCE dissolution rate is proportional to  $Re_a$ , or equivalently to the acoustically induced oscillatory pore water velocity. This is in agreement with previous studies suggesting that NAPL dissolution rates depend on the interstitial pore water velocity (Powers et al., 1994; Zhou et al., 2000; Chrysikopoulos, 1995; Bao et al., 2003; Seagren and Moore, 2003).

It should be noted that the predicted values of  $Re_a$  as a function of  $p_s$  (Figure 2c) are greater for the larger bead-size

**Table 2. Experimental Effluent TCE Concentrations**

$\phi$ (Hz)	$p_s$ (Pa)	1 mm Beads		2 mm Beads	
		$\bar{C}_b$ (mg/L)	$\bar{C}_a$ (mg/L)	$\bar{C}_b$ (mg/L)	$\bar{C}_a$ (mg/L)
75	812	52.85	53.41	24.79	31.07
125	812	51.56	52.67	20.84	23.43
161	812	38.36	72.53	23.55	39.17
200	812	54.99	57.62	35.56	37.38
225	812	44.01	96.73	28.74	56.35
245	812	38.99	63.60	27.97	37.71
245	812	—	—	34.23	45.47
275	812	70.40	55.69	19.05	20.11
276	812	—	—	31.51	32.77
285	812	50.55	81.51	25.57	37.09
245	488	—	—	32.04	35.86
245	1008	48.91	84.36	29.97	49.18
245	1235	53.31	80.85	21.12	28.52
245	1625	58.21	121.42	32.52	72.01

column packing, whereas the experimental results indicate that the observed percent changes in effluent concentrations as a function of  $p_s$  (Figure 6), and as a function of  $Re_a$  (Figure 7) are greater for the smaller bead size column packing. This inconsistency may be attributed to greater DNAPL-water interfacial areas associated with the smaller bead column packing (Powers et al., 1994). Individual pore spaces are smaller for the smaller bead column packing, thus, DNAPL blobs are spread into more pore spaces leading to larger DNAPL-water interfacial areas and larger mass-transfer rates. Consequently,  $\Delta C$  for the smaller bead-size column packing is influenced more by the acoustic waves that cause an oscillatory pore water velocity at the DNAPL-water interface.

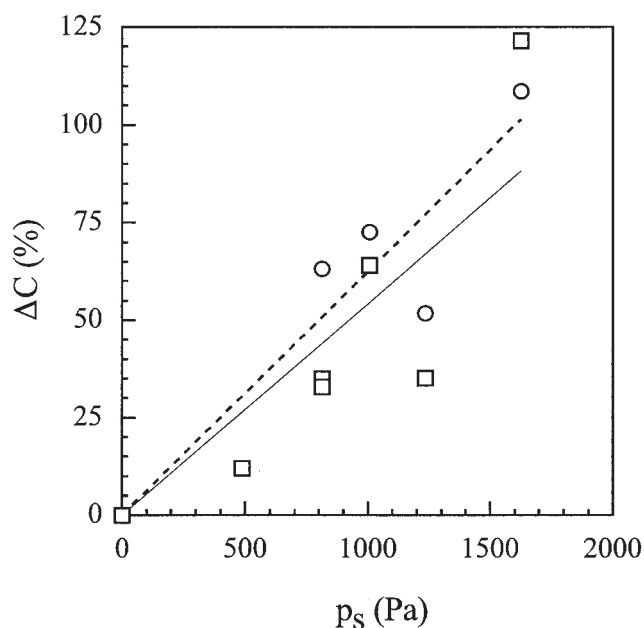


**Figure 6. Percent change in effluent dissolved TCE concentration as a function of  $p_s$  (here  $x=0.15$  m,  $\phi=245$  Hz).**

Circles with best fit dashed lines and squares with best fit solid lines represent column packings of 1 and 2 mm size beads, respectively.

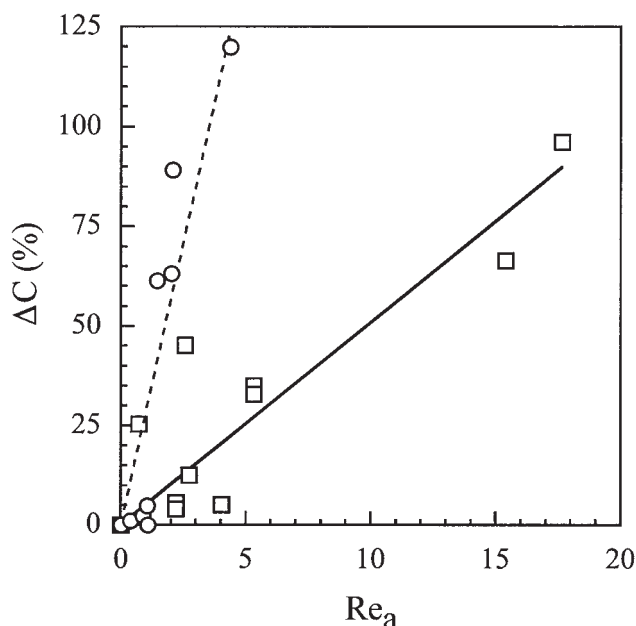


**Figure 7. Percent change in effluent concentration as a function of  $Re_a$  at  $x = 15$  cm.**

Circles with best fit dashed lines and squares with best fit solid lines represent column packings of 1 and 2 mm size beads, respectively.

## Summary

The effect of acoustic pressure waves on TCE ganglia dissolution in a water saturated column packed with glass beads is examined theoretically and experimentally. A mathematical model is developed to determine the acoustically induced pore fluid displacement relative to the solid matrix displacement. The acoustic Reynolds number is predicted to decrease almost exponentially with increasing  $x$ , reach an asymptotic value with increasing  $\phi$ , and increase linearly with increasing  $p_s$ . The experimental TCE dissolution data show that the oscillatory pore water velocity caused by acoustic pressure waves can lead up to a 120% increase in the effluent dissolved TCE concentrations under specific conditions. The increase in effluent concentrations is found to be proportional to the applied acoustic source pressure. Although  $Re_a$  values are predicted to be greater for the column packed with larger beads, acoustically enhanced TCE dissolution is found to be greater in the column packed with smaller glass beads. This is due to greater TCE-water interfacial areas associated with the smaller bead size column packing. The effect of acoustic waves on DNAPL dissolution is limited by the distance from the acoustic source and the amount of acoustic pressure that can be generated at the source. The results presented here are valid only for TCE dissolution in homogeneous porous media and may differ for more soluble DNAPLs and heterogeneous porous media. Further investigations are required to fully understand resonant behavior of saturated porous media and the theoretical relationship between  $Re_a$  and DNAPL dissolution. However, the results of this study indicate that the use of acoustic pressure waves, complementing traditional pump-and-treat methodology, may be a viable method to decrease remediation times and costs for DNAPL contaminated aquifers.

## Notation

- $A_1, \dots, A_4$  = Laplace domain constants  
 $C$  = dissolved phase DNAPL concentration (solute mass/liquid volume) ( $M/L^3$ )  
 $\bar{C}_a$  = mean concentration in the presence of acoustic waves,  $M/L^3$   
 $\bar{C}_b$  = mean base case concentration,  $M/L^3$   
 $\Delta C$  = percent change in concentration, %  
 $d$  = mean grain size diameter of the porous medium, L  
 $f(t)$  = time-dependent source function,  $F/L^2t$   
 $G$  = defined in Eq. 43  
 $H$  = Heaviside unit step function  
 $I_0$  = modified Bessel function of zero-order  
 $K$  = hydraulic conductivity, L/t  
 $m$  = vector of Laplace transformed dependent variables  
 $m_0$  = function of transformed variable  $i$   
 $p$  = fluid pressure,  $F/L^2$   
 $p_e$  = column effluent fluid pressure,  $F/L^2$   
 $p_s$  = acoustic source fluid pressure,  $F/L^2$   
 $q_1, \dots, q_4$  = eigenvectors, defined in Eqs. 26–28  
 $Q$  = defined in Eq. 42  
 $Re_a$  = acoustic Reynolds number defined in Eq. 47  
 $S$  = fluid-solid viscous drag coefficient defined in Eq. 4,  $L/t$   
 $t$  = time, t  
 $U_r$  = relative pore water velocity, L/t  
 $U_{r,a}$  = oscillatory pore water velocity amplitude, L/t  
 $X$  = longitudinal spatial coordinate, L

## Greek letters

- $\alpha_1, \dots, \alpha_4$  = eigenvalues, defined in Eqs. 21–23  
 $\beta$  = dummy variable  
 $\gamma$  = specific fluid weight,  $F/L^3$   
 $\eta$  = kinematic fluid viscosity,  $L^2/t$   
 $\theta$  = porosity (liquid volume/aquifer volume),  $L^3/L^3$   
 $\lambda$  = solid matrix Lamé constant,  $F/L^2$   
 $\Lambda$  = defined in Eq. 41  
 $\mu$  = solid matrix Lamé constant,  $F/L^2$   
 $v$  = Laplace transform parameter  
 $\xi_s$  = solid displacement, L  
 $\xi_f$  = fluid displacement, L  
 $\xi_r$  = fluid displacement relative to solid displacement, L  
 $\rho_{solid}$  = glass bead density,  $M/L^3$   
 $\rho_f$  = fluid bulk density,  $M/L^3$   
 $\rho_{H_2O}$  = density of water,  $M/L^3$   
 $\rho_s$  = bulk density of the solid matrix,  $M/L^3$   
 $\sigma$  = solid stress,  $F/L^2$   
 $\tau$  = dummy integration variable  
 $\phi$  = acoustic wave frequency,  $1/t$   
 $\omega$  = angular frequency  
 $\Omega_1, \Omega_2$  = defined in Eq. 24 and 25, respectively

## Acknowledgments

This work was funded by the University of California Water Resources Center Project W-938 and NSF Award Number BES-0329398. The content of this manuscript does not necessarily reflect the views of the agencies, and no official endorsement should be inferred. The authors also gratefully acknowledge the laboratory assistance of Jo Ann Dacanay and Julio S. Fernandez.

## Literature Cited

- Abramowitz, M., I. A. Stegun, *Handbook of Mathematical Functions*, National Bureau of Standards, Washington, DC (1965).  
 Bao, W. M. J., E. T. Vogler, and C. V. Chrysikopoulos, "Nonaqueous Phase Liquid Pool Dissolution in Three-Dimensional Heterogeneous Subsurface Formations," *Environ. Geol.*, **43**, 968 (2003).  
 Biot, M. A., "Theory of Propagation of Elastic Waves in a Fluid-Filled Porous Solid. I. Low-Frequency Range," *J. Appl. Phys.*, **28**(2), 168 (1956a).  
 Biot, M. A., "Theory of Propagation of Elastic Waves in a Fluid-Filled Porous Solid. II. High-Frequency Range," *J. Appl. Phys.*, **28**(2), 179 (1956b).

- Brandes, D., and K. J. Farley, "Importance of Phase Behavior on the Removal of Residual DNAPLs from Porous Media by Alcohol Flooding," *Water Environ. Res.*, **65**(7), 869 (1993).
- Chatzis, I., N. R. Morrow, and H. T. Lim, "Magnitude and Detailed Structure of Residual Oil Saturation," *Soc. Pet. Eng. J.*, **24**, 311 (1983)
- Chaudhry, G. R., *Biological Degradation and Bioremediation of Toxic Chemicals*. Dioscorides Press, Portland, OR (1994).
- Chrysikopoulos, C. V., "Three-Dimensional Analytical Models of Contaminant Transport from Nonaqueous Phase Liquid Pool Dissolution in Saturated Subsurface Formations," *Water Resour. Res.*, **31**(4), 1137 (1995).
- Chrysikopoulos, C. V., E. A. Voudrias, and M. M. Fyrrillas, "Modeling of Contaminant Transport Resulting from Dissolution of Nonaqueous phase Liquid Pools in Saturated Porous Media," *Transp. Porous Media*, **16**, 125 (1994).
- Chrysikopoulos, C. V., K. Y. Lee, and T. C. Harmon, "Dissolution of a Well-Defined Trichloroethylene Pool in Saturated Porous Media: Experimental Design and Aquifer Characterization," *Water Resour. Res.*, **36**(7), 1687 (2000).
- Chrysikopoulos, C. V., P.-Y. Hsuan, M. M. Fyrrillas, and K. Y. Lee, "Mass Transfer Coefficient and Concentration Boundary Layer Thickness for a Dissolving NAPL Pool in Porous Media," *J. Hazardous Materials*, **B97**, 245 (2003).
- de Boer, R., and W. Ehlers, "Uplift Friction and Capillarity - Three Fundamental Effects for Liquid-Saturated Porous Solids," *Int. J. Solids Structures*, **26**, 43 (1990).
- de Boer R., W. Ehlers, and Z. Liu, "One-Dimensional Transient Wave Propagation in Fluid-Saturated Incompressible Porous Media," *Archive Appl. Mechanics*, **63**, 59 (1993).
- de Klerk, A., "Voidance Variation in Packed Beds at Small Column to Particle Diameter Ratio," *AIChE J.*, **49**(8), 2022 (2003).
- Dela Barre, B. K., T. C. Harmon, and C. V. Chrysikopoulos, "Measuring and Modeling the Dissolution of Nonideally Shaped Dense Nonaqueous Phase liquid Pools in Saturated Porous Media," *Water Resour. Res.*, **38**(8), 8-1 (2002).
- Dusseault, M., B. Davidson, and T. Spanos, "Pressure Pulsing: The Ups and Downs of Starting a New Technology," *J. Canadian Petrol. Technol.*, **39**(4), 13 (2000).
- Fortin, J., W. A. Jury, and M. A. Anderson, "Enhanced Removal of Trapped Non-Aqueous Phase Liquids from Saturated Soil Using Surfactant Solutions," *J. Contam. Hydrol.*, **24**(3-4), 247 (1997).
- Ha, M. Y., and S. A. Yavuzkurt, "Theoretical Investigation of Acoustic Enhancement of Heat and Mass Transfer-I. Pure Oscillating Flow," *Int. J. Heat Mass Transfer*, **36**(8), 2183 (1993a).
- Ha, M. Y., and S. A. Yavuzkurt, "Theoretical Investigation of Acoustic Enhancement of Heat and Mass Transfer-II. Oscillating Flow with a Steady Velocity Component," *Int. J. Heat Mass Transfer*, **36**(8), 2193 (1993b).
- Imhoff, P. T., P. R. Jaffe, and G. G. Pinder, "An Experimental Study of Complete Dissolution of Nonaqueous Phase Liquid in Saturated Porous Media," *Water Resour. Res.*, **30**, 307 (1994).
- IMSL, *IMSL MATH/LIBRARY user's manual 2.0*. Houston: IMSL (1991).
- Khachikian, C., and T. C. Harmon, "Nonaqueous Phase Liquid Dissolution in Porous Media: Current State of Knowledge and Research Needs," *Transp. Porous Media*, **38**, 3 (2000).
- Lee, K. Y., and C. V. Chrysikopoulos, "Dissolution of a Well-Defined Trichloroethylene Pool in Saturated Porous Media: Experimental Results and Model Simulations," *Water Res.*, **36**, 3911 (2002).
- Mason, A. R., and B. H. Kueper, "Numerical Simulation of Surfactant-Enhanced Solubilization of Pooled DNAPL," *Environ. Sci. Technol.*, **30**(11), 3205 (1996)
- Mercer, J. W., and R. M. Cohen, "A Review of Immiscible Fluids in the Subsurface: Properties, Model Characterization and Remediation," *J. Contam. Hydrol.*, **6**, 107 (1990).
- Mohanty, K. K., H. T. Davis, and L. E. Scriven, "Physics of Oil Entrapment in Water Wet Rocks," *Soc. Pet. Eng. Reservoir Eng.*, **2**, 113 (1987).
- Morrow, N. R., I. Chatzis, and J. J. Taber, "Entrapment and Mobilization of Residual Oil in Bead Packs," *Soc. Pet. Eng. Reservoir Eng.*, **3**, 211 (1988).
- Nambi, I. M., and S. E. Powers, "Mass Transfer Correlations for Nonaqueous Phase Liquid Dissolution from Regions with High Initial Saturations," *Water Resour. Res.*, **39**(2), 1030 (2003).
- Pan, Y., and R. N. Horne, "Resonant Behavior of Saturated Porous Media," *J. Geophys. Res.*, **105**(B5), 11021 (2000).
- Pennel, K. D., L. M. Abriola, and W. J. Weber, Jr., "Surfactant-Enhanced Solubilization of Residual Dodecane in Soil Columns. 1. Experimental Investigation," *Environ. Sci. Technol.*, **27**, 2332 (1993).
- Pennel, K. D., L. M. Abriola, and W. J. Weber, Jr., "An Experimental Investigation of NAPL Dissolution in Saturated Subsurface Systems: Transient Mass Transfer Rates," *Water Resour. Res.*, **30**(2), 321 (1994).
- Reddi, L. N., S. Menon and A. Plant, "Pore-Scale Investigations on Vibratory Mobilization of LNAPL Ganglia," *J. Hazardous Materials*, **62**, 211 (1998).
- Reddi, L. N., and H. Wu, "Mechanisms Involved in Vibratory Destabilization of NAPL Ganglia in Sands," *J. Environ. Eng.*, **122**(12), 1115 (1996).
- Roberts, P. M., and A. Sharma, V. Uddameri, M. Monagle, D. E. Dale, and L. K. Steck, "Enhanced DNAPL Transport in a Sand Core During Dynamic Stress Simulation," *Environ. Eng. Sci.*, **18**(2), 67 (2001).
- Seagren, E. A., B. E. Rittmann, and A. J. Valocchi, "Quantitative Evaluation of the Enhancement of NAPL-Pool Dissolution by Flushing and Biodegradation," *Environ. Sci. Technol.*, **28**(5), 833 (1994).
- Seagren, E. A., T. O. Moore., "Nonaqueous Phase Liquid Pool Dissolution as a Function of Average Pore Water Velocity," *J. Environ. Eng. (ASCE)*, **129**(9), 786 (2003).
- Tatalovich, M. E., K. Y. Lee, and C. V. Chrysikopoulos, "Modeling the Transport of Contaminants Originating From the Dissolution of DNAPL Pools in Aquifers in the Presence of Dissolved Humic Substances," *Transp. Porous Media*, **38**, 93 (2000).
- Vogler, E. T., and C. V. Chrysikopoulos, "Experimental Investigation of Acoustically Enhanced Solute Transport in Porous Media," *Geophysical Res. Letters*, **29**(15), 5-1 (2002).
- Wilson, J. L., S. H. Conrad, W. R. Mason, and W. Peplinski, "Laboratory Investigation of Residual Liquid Organics from Spills, Leaks, and the Disposal of Hazardous Wastes in Groundwater," U.S. EPA, EPA/600/6-0/004, Narragansett, RI (1990).
- Zhou, D., L. A. Dillard, and M. J. Blunt., "A Physically Based Model of Dissolution of Nonaqueous Phase Liquids in the Saturated Zone," *Transp. Porous Media*, **39**, 227 (2000).
- Zimmerman C., and M. Stern, "Analytical Solutions for Harmonic Wave Propagation in Poroelastic Media," *J. Eng. Mech.*, **120**(10), 2154 (1994).

Manuscript received Jan. 13, 2004, and revision received Mar. 10, 2004.